DESY 04-013
January 2004

Terawatt-scale sub-10-fs laser technology – key to generation of GW-level attosecond pulses in X-ray free electron laser

E.L. Saldin, E.A. Schneidmiller, and M.V. Yurkov

Deutsches Elektronen-Synchrotron (DESY), Hamburg, Germany

Abstract

We propose a technique for the production of attosecond X-ray pulses which is based on the use of X-ray SASE FEL combined with a femtosecond laser system. A few-cycle optical pulse from a Ti:sapphire laser interacts with the electron beam in a two-period undulator resonant to 800 nm wavelength and produces energy modulation within a slice of the electron bunch. Following the energy modulator the electron beam enters the X-ray undulator and produces SASE radiation. Due to energy modulation the frequency is correlated to the longitudinal position within the few-cycle-driven slice of SASE radiation pulse. The largest frequency offset corresponds to a single-spike pulse in the time domain which is confined to one half-oscillation period near the central peak electron energy. The selection of single-spike pulses is achieved by using a crystal monochromator after the X-ray undulator. Our studies show that the proposed technique is capable to produce 300 attoseconds long single pulses with GW-level output power in the 0.1 nm wavelength range, and is applicable to the European X-Ray Laser Project XFEL and the Linac Coherent Light Source at SLAC.

1 Introduction

At the start of this century, we have seen a revolution in synchrotron radiation source intensities. This revolution stemmed from the technique of free electron laser (FEL) based on self-amplified spontaneous emission (SASE), combined with recent progress in accelerator technologies, developed in connection with high-energy linear colliders. In 2001, the VUV FEL at the TESLA Test Facility at DESY (Hamburg, Germany) has successfully demonstrated saturation from 82 nm to 125 nm with GW-level peak power and pulse duration down to 40 fs [1,2]. It is the first result from this device that Wabnitz et al. reported in [3]. They illuminated xenon clusters with high-intensity (10^{14} W/cm^2) VUV FEL pulses and observed an unexpectedly strong absorption of the VUV radiation. Such a highly nonlinear optical interaction between light and matter at VUV wavelength range has never been seen before and these fascinating results show the potential of this new class of light sources for scientific research. While modern third generation synchrotron light sources are reaching their fundamental performance limit, recent successes in the development of the VUV FEL at DESY have paved the way for the construction of the novel type of light source which will combine most of the positive aspects of both a laser and a synchrotron. Starting in 2004, the phase 2 extension of TTF will deliver FEL radiation down to the soft X-ray spectral range with minimum wavelength of about 6 nm in the first harmonic and reaching into "water window" in the second harmonic [4].

Recently the German government, encouraged by these results, approved funding a hard X-ray SASE FEL user facility – the European X-Ray Laser Project XFEL. The US Department of Energy (DOE) has given SLAC the goahead for engineering design of the Linac Coherent Light Source (LCLS) device to be constructed at SLAC. These devices should produce 100 fs X-ray pulses with over 10 GW of peak power [5,6]. These new X-ray sources will be able to produce intensities of the order of 10^{18} W/cm^2. The main difference between the two projects is the linear accelerator, an existing room temperature linac for LCLS at SLAC, and a future superconducting linac for European XFEL. The XFEL based on superconducting accelerator technology will make possible not only a jump in a peak brilliance by ten orders of magnitude, but also an increase in average brilliance by five orders of magnitude compared to modern 3rd generation synchrotron radiation facilities. The LCLS and European XFEL projects are scheduled to start operation in 2008 and 2012, respectively.

The motivation for the development of XFELs was recently described in detail in [5,6]. The discussion in the scientific community over the past decade has produced many ideas for novel applications of the X-ray laser. Brilliance, coherence, and timing down to the femtosecond regime are the three properties which have the highest potential for new science to be explored with

an XFEL. In its initial configuration the XFEL pulse duration is about 100 femtoseconds. Even though this is a few hundreds times shorter than in third generation light sources, it can probably be further reduced to about 10 femtoseconds [7–9]. A novel way to generate sub-10 fs x-ray pulses – the slotted spoiler method (P. Emma, 2003) has been proposed recently. This method is based on spoiling the beam phase density in a part of the electron bunch so that this part will not lase, while preserving lasing in a short length of the bunch. The FEL performance of the spoiled beam approach was computed using the time-dependent GENESIS simulation. It has been shown that it is possible to produce X-ray pulses with duration of 3-4 fs FWHM for nominal LCLS bunch compression parameters [10].

Femtosecond-resolution experiments with X-rays can possibly show directly how matter is formed out of atoms. In fact, X-ray pulse duration even shorter than one femtosecond may be useful for many scientific applications. The reason is that phenomena inside atoms occur on sub-femtosecond timescale. Generating single attosecond $\sim$ 0.1 nm X-ray pulses is one of the biggest challenges in physics. The use of such a tool will enable to trace process inside the atoms for the first time. If there is any place where we have a chance to test the main principles of quantum mechanics in the pure way, it is there.

The interest in the science with attosecond pulses is growing rapidly in the very large laser community. This community is familiar with attosecond pulses of light at photon energies up to about 0.5 keV (3 nm). This is achieved by focusing a fs laser into a gas target creating radiation of high harmonics of fundamental laser frequency. The key to these developments was the invention of laser systems delivering pulses in the range of 5 fs with pulse energies higher than a fraction of mJ. This approach produced the first measurable XUV pulses in the 200 as regime [11,12]. In principle, table-top ultra-fast X-ray sources have the right duration to provide us with a view of subatomic transformation processes. However, their power and photon energy are by far low. The XFEL is ideally suited the purpose of this emerging field of science. Recently an approach for the generation of attosecond pulses combining fs quantum laser and harmonic cascade (HC) FEL scheme [13,14] was proposed in [15]. The HC FEL scheme has the potential to produce coherent light down to wavelengths of a few nm in an undulator sequence [16]. The analysis presented in [15] shows that this technique has potential to produce 100 as long radiation pulses with MW-level of output power down to 1 nm wavelength.

The X-ray SASE FEL holds a great promise as a source of radiation for generating high power, single attosecond pulses. What ultimately limits the XFEL pulse duration? Since the temporal and spectral characteristics of the radiation field are related to each other through Fourier transform, the bandwidth of the XFEL and the pulse duration cannot vary independently of each other. There is a minimum duration-bandwidth product (uncertainty principle). The

shortest possible X-ray pulse duration generated by XFEL is limited by the intrinsic bandwidth of the SASE process. In the case of the European XFEL and the LCLS, the FWHM bandwidth near saturation (at 0.1 nm) is about 0.1%, indicating a 300-as coherence time determined by the bandwidth product. Recently a scheme to achieve pulse durations down to 400-600 attoseconds at a wavelength of 0.1 nm has been proposed [17]. It uses a statistical properties of SASE FEL high harmonic radiation. The selection of a single 10-GW level attosecond pulses is achieved by using a special trigger in data acquisition system. A promising scheme for attophysics experiments using this approach has been studied and could be implemented in the XFEL design [18].

In this paper we propose a new method allowing to reduce the pulse length of the X-ray SASE FEL to the shortest conceptual limit of about 300 as. It is based on the application of a sub-10-fs laser for slice energy modulation of the electron beam, and application of a crystal monochromator for the selection of single attosecond pulses with GW-level output power.

2 The principle of attosecond techniques based on the use of XFEL combined with fs quantum laser

A basic scheme of the attosecond X-ray source is shown in Fig. 1. An ultrashort laser pulse is used to modulate the energy of electrons within the femtosecond slice of the electron bunch at the seed laser frequency. The seed laser pulse will be timed to overlap with the central area of the electron bunch. It serves as a seed for a modulator which consists of a short (a few periods) undulator. Following the energy modulator the beam enters the X-ray undulator. The process of amplification of radiation in this undulator develops in the same way as in a conventional X-ray SASE FEL: fluctuations of the electron beam current serve as the input signal [19]. The proposed scheme for the generation of attosecond pulses is based on frequency-chirping the SASE radiation

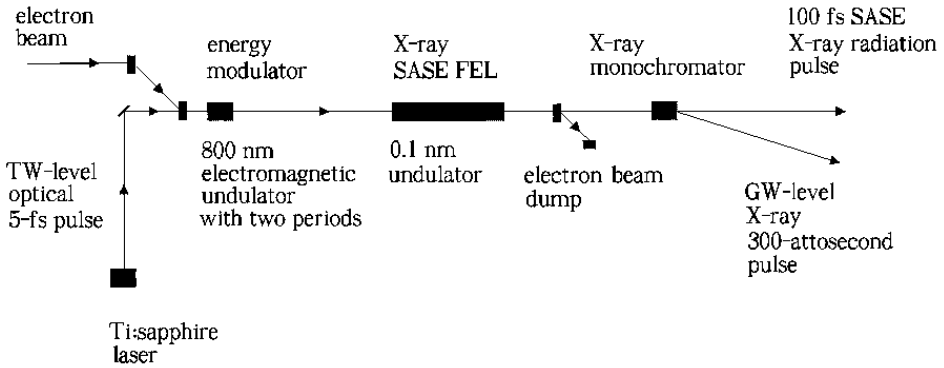

Fig. 1. Schematic diagram of attosecond X-ray source

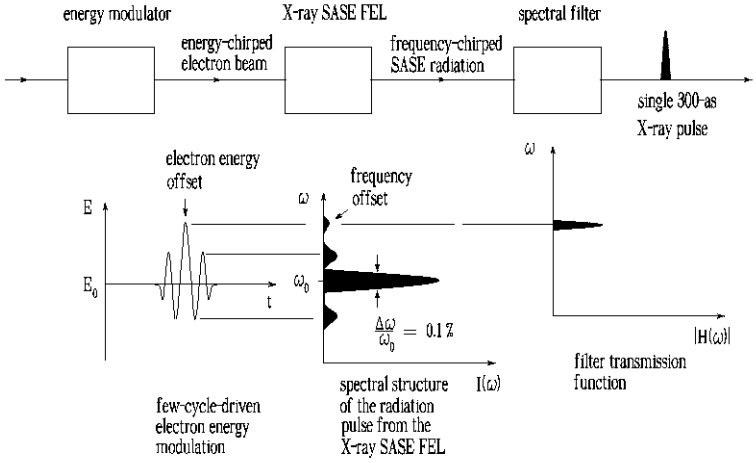

Fig. 2. Sketch of single attosecond X-ray pulse synthesation through frequency chirping and spectral filtering

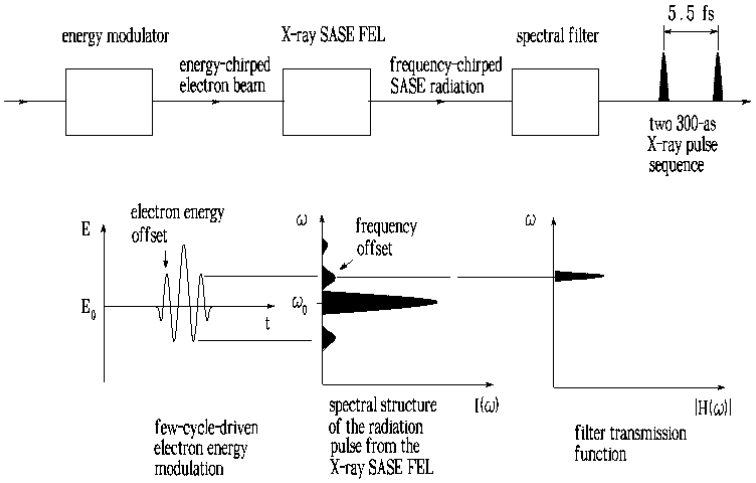

Fig. 3. Sketch of two attosecond X-ray pulse sequence synthesation through frequency chirping and spectral filtering. Pulse separation is $2T_0$, where T_0 is the Ti:sapphire laser oscillation period

pulse. When an electron beam traverses an undulator, it emits radiation at the resonance wavelength $\lambda = \lambda_{\rm w}(1 + K^2/2)/(2\gamma^2)$. Here $\lambda_{\rm w}$ is the undulator period, $mc^2\gamma$ is the electron beam energy, and K is the undulator parameter. The laser-driven sinusoidal energy chirp produces a correlated frequency chirp of the resonant radiation $\delta\omega/\omega \simeq 2\delta\gamma/\gamma$. After the undulator, the radiation is passed through a crystal monochromator which reflects a narrow bandwidth. Since the radiation frequency is correlated to the longitudinal position within the beam, a short temporal radiation pulse is transmitted through the monochromator.

Recent technological advances in ultrafast optics have permitted the generation of optical pulses comprising only a few oscillation cycles of the electric

and magnetic fields. The pulses are delivered in a diffraction-limited beam [20]. The combination of a X-ray SASE FEL and a few-cycle laser field techniques is very promising. Our concept of an attosecond X-ray facility is based on the use of a few-cycle optical pulse from a Ti:sapphire laser system. This optical pulse is used for the modulation of the energy of the electrons within a slice of the electron bunch at a wavelength of 800 nm. Due to the extreme temporal confinement, moderate optical pulse energies of the order of a few mJ can result in an electron energy modulation amplitude larger than 30-40 MeV. In few-cycle laser fields high intensities can be "switched on" nonadiabatically within a few optical periods. As a result, a central peak electron energy modulation is larger than other peaks. This relative energy difference is used for the selection of SASE radiation pulses with a single spike in the time domain by means of a crystal monochromator. A schematic, illustrating these processes, is shown in Fig. 2. Many different output fields can be realized by using different spectral windowing. For instance, it is possible to generate a sequence of 300-as X-ray pulses, separated by T_0 (or $2T_0$), where T_0 is the Ti:sapphire laser oscillation period. Such operation of the attosecond X-ray source is illustrated in Fig. 3.

The discussion in this paper is focused on the parameters for the European XFEL operating in the wavelength range around 0.1 nm [5]. Optimization of the attosecond SASE FEL has been performed with the three-dimensional, time dependent code FAST [21] taking into account all physical effects influencing the SASE FEL operation (diffraction effects, energy spread, emittance, slippage effect, etc.). In our scheme the separation of the frequency offset from the central frequency by a monochromator is used to distinguish the 300-as pulse from the 100 fs intense SASE pulse. The monochromatization is straightforward: for the 0.1 nm wavelength range, Bragg diffraction is the main tool used for such purposes. In this case, one has to take care that the short pulse duration is preserved. Transmission through the monochromator will produce some intrinsic spreading of the pulse, and the minimum pulse duration which may be selected by this method is limited by the uncertainty principle. The number of possible reflections which provide the required spectral width is rather limited. We are discussing here only Ge crystals, which have the largest relative bandwidth. This is an important feature which ensures the preservation of the single-spike pulse duration. In its simplest configuration the monochromator consists of Ge crystal diffracting from the (111) lattice planes. We show that it is possible to produce X-ray pulses with FWHM duration of 300 as. In some experimental situations this simplest configuration of monochromator is not optimal. In particular, our study has shown that the maximum contrast of the attosecond X-ray pulses does not exceed 80% and is due to the long tail of the intrinsic crystal reflectivity curve. The obvious and technically possible solution of the problem of contrast increase might be to use a premonochromator. One can align the premonochromator so that the main peak of the spectrum is blocked.

3 Generation of attosecond pulses from XFEL

In the following we illustrate the operation of an attosecond SASE FEL for the parameters close to those of the European XFEL operating at the wavelength 0.1 nm [5]. The parameters of the electron beam are: energy 15 GeV, charge 1 nC, rms pulse length 25 μm, rms normalized emittance 1.4 mm-mrad, rms energy spread 1 MeV. Undulator period is 3.4 cm.

3.1 Slice modulation of the electron beam

The parameters of the seed laser are: wavelength 800 nm, energy in the laser pulse 2–4 mJ, and FWHM pulse duration 5 fs (see Fig. 4). The laser beam is focused onto the electron beam in a short undulator resonant at the optical wavelength of 800 nm. Parameters of the undulator are: period length 50 cm, peak field 1.6 T, number of periods 2.

Optimal conditions of the focusing correspond to the positioning of the laser beam waist in the center of the undulator. In laser pulses comprising just a few wave cycles, the amplitude envelope and the carrier frequency are not sufficient to characterize and control laser radiation, because the evolution of the light field is also influenced by a shift of the carrier wave with respect to the pulse peak [20]. Recently, the generation of intense, few-cycle laser pulses with a stable carrier envelope phase φ_0 was demonstrated [22]. Let us consider the principle question for the design of few-cycle pulse experiments: how does the pulse phase behave during linear propagation? In order to answer

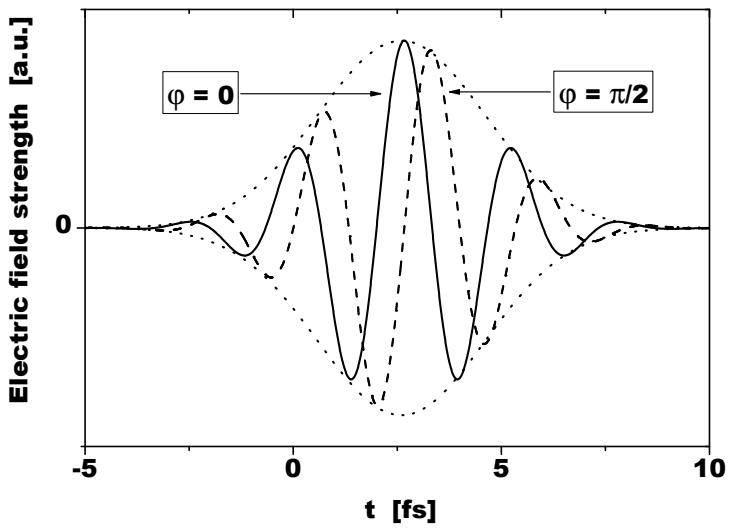

Fig. 4. Possible evolutions of the electric field in the 5-fs pulse. carried at a wavelength 800 nm for two different pulse phases ($\phi = 0, \pi/2$)

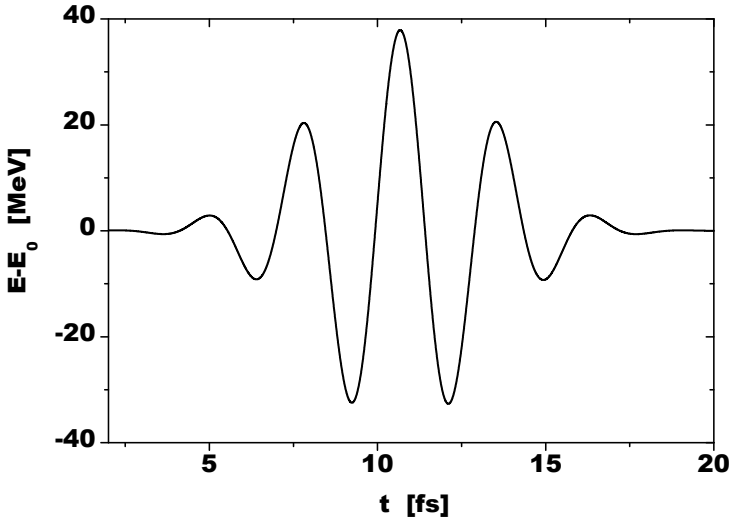

Fig. 5. Energy modulation of the electron beam at the exit of the modulator undulator. The laser parameters are $\lambda = 800$ nm, $W_{\rm peak} = 800$ GW, and FWHM pulse duration of $\tau_{\rm p} = 5$ fs

this question, we can calculate the evolution of few-cycle pulses in vacuum, which is most conveniently described by a parabolic wave equation and by starting from a Gaussian initial spatial pulse profile [20]. Choosing the initial pulse phase to be φ_0 at the beam waist, one reveals that the carrier envelope phase in the far field $\varphi(\infty) = \varphi_0 - \pi/2$ undergoes a phase shift due to the Guoy phase shift $-\pi/2$ [20]. Note that the Guoy phase shift and all the other changes experienced by the pulse during propagation do not depend on the initial phase φ_0.

For an attosecond X-ray source it is of great interest to maximize the central peak energy offset, which depends sensitively on the absolute phase of the seed laser pulse φ_0. We start with an illustration of the few-cycle-driven energy modulation assuming that the peak electric field appears at the peak of the envelope when the laser pulse passes the undulator center (i.e. $\varphi_0 = 0$ at the Gaussian beam waist). The interaction with the laser light in the undulator then produces a time dependent electron energy modulation as shown in Fig. 5. For the laser (FWHM) pulse duration of 5 fs at a laser pulse energy 2-4 mJ, we expect a central peak energy modulation 30-40 MeV.

3.2 Monochromator

The width of the spectral distribution of the SASE radiation will be determined by the frequency chirp, provided the frequency chirp is larger than FEL bandwidth. A monochromator may be used to select the pulses of short duration, due to correlation between frequency and longitudinal position in the radiation pulse. For 12 keV photons, we consider Bragg diffraction in crystals

as a method of bandwidth selection. Special attention is called to the fact that the relative spectral width for the given Bragg reflection is independent of the wavelength or glancing angle of X-rays and is given merely by properties of the crystal and the reflecting atomic planes. In particular, it implies that the choice of a crystal and reflecting atomic planes determines the spectral resolution. For example, one can consider Si(111) crystals, which have a FWHM bandwidth of $\Delta\lambda/\lambda = 1.3 \times 10^{-4}$, or Ge(111)crystals, which have a FWHM bandwidth of $\Delta\lambda/\lambda = 3.4 \times 10^{-4}$. Monochromators at synchrotron beam lines are most commonly fabricated from silicon. The reason is that the semiconductor industry has created a huge demand for defect-free , perfect single crystals. Silicon is by no means the only choice, and in recent years diamond has become a popular alternative, due to the fact it has the highest thermal conductivity and low absorption.

An attosecond X-ray source requires a relatively broadband monochromator. The larger the monochromator bandwidth is, the shorter the minimal pulse duration than can be extracted. We are discussing here only Germanium single crystals which have the largest relative bandwidth. Although Ge is not as perfect as silicon or diamond, sufficiently large perfect Ge crystals are available today. For 12 keV photons Bragg peaks of Ge crystals have reflectivities of approximately 75%. Figure 6 gives an example of a reflectivity curve for a thick absorbing crystal. The drawing of Fig. 6 shows several interesting features. The shape is asymmetric and is due to absorption effect. The tails of the reflectivity curve decrease as $(\Delta\lambda/\lambda)^{-2}$. It should be pointed out that the tail of reflectivity curve plays important role in the operation of the attosecond X-ray source, and this characteristic of spectral window and attosecond pulse contrast are ultimately connected. Good crystal quality is required for

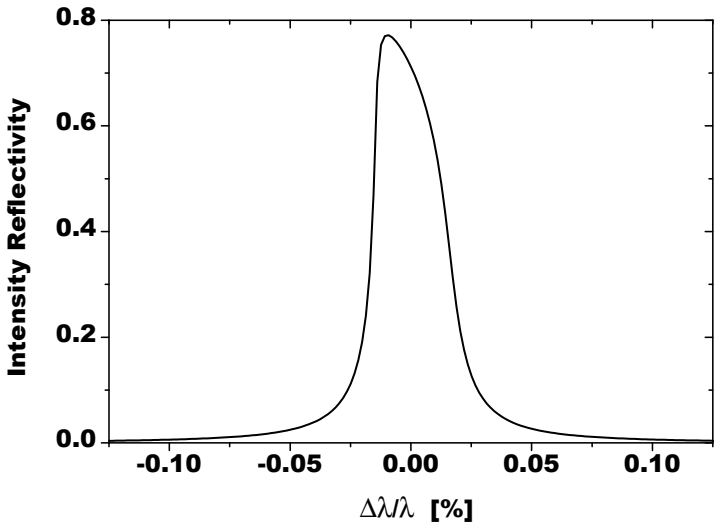

Fig. 6. Reflectivity curve for a thick absorbing crystal in the Bragg case. Germanium, 111, 0.1 nm

high resolving power. Similarly, a good resolving power requires a collimated beam. In fact, the angular spread of an insufficiently collimated beam negatively affects the wavelength resolution just like poor crystal quality. The Ge monochromator angular acceptance is of order 50 μrad for a wavelength 0.1 nm, and is well matched to the natural opening angle, (1 μrad), of an XFEL source. Therefore, a crystal monochromator works better with XFEL radiation than with conventional synchrotron source.

Besides the crystal quality, other factors must be considered in selecting a scheme for a monochromator. The monochromator crystal must be thermally stable and capable of being exposed to XFEL output radiation with limited radiation damage. We have chosen the one Ge (111) crystal scheme of the X-ray monochromator with silicon premonochromator, which withdraws the major heat load from the actual short pulse selection Ge monochromator. We consider Laue diffraction in Si crystals as a method of bandwidth selection in premonochromator. In the pre-monochromator part one can use ten Si crystal plates of 15μm thickness and the reflection Si(111). Given the crystal plate is perfect, it reflects 90% of the incident X-rays within a band of $\Delta\lambda/\lambda \simeq 10^{-4}$. One can align the Si plates so that the main peak of the spectrum is blocked. The radiation power which reaches the broadband (Ge) monochromator crystal is 10% of the initial value. Only 30% of the offset frequency radiation is absorbed in ($15 \times 10 = 150\mu$m thickness) premonochromator totally, and the rest passes through. Another advantage of the premonochromator is the possibility to increase the contrast of output attosecond X-ray pulses.

3.3 Output characteristics of attosecond FEL

A complete description of the X-ray FEL can be performed only with three-dimensional, time-dependent numerical simulation code. Since amplification process starts from shot noise, properties of a single-spike selection should be described in statistical term. The statistics of concern are defined over an ensemble of radiation pulses.

In the present scheme an electron beam with slice modulation of the energy passes through the undulator and produces SASE radiation. Since only a small fraction of the bunch is modulated (10 fs versus 200 fs of FWHM electron pulse duration, see Fig.5), the total energy in the radiation pulse remains approximately the same as in the case of nonmodulated electron beam (see Fig. 7), and saturation is achieved at an undulator length of about 120 m. Figure 8 shows typical temporal and spectral structure of the radiation pulse at saturation. In the present numerical example the central part of the electron bunch was subjected to the slice energy modulation, and one can notice its clear signature in the temporal structure. Figure 9 shows an enlarged view of

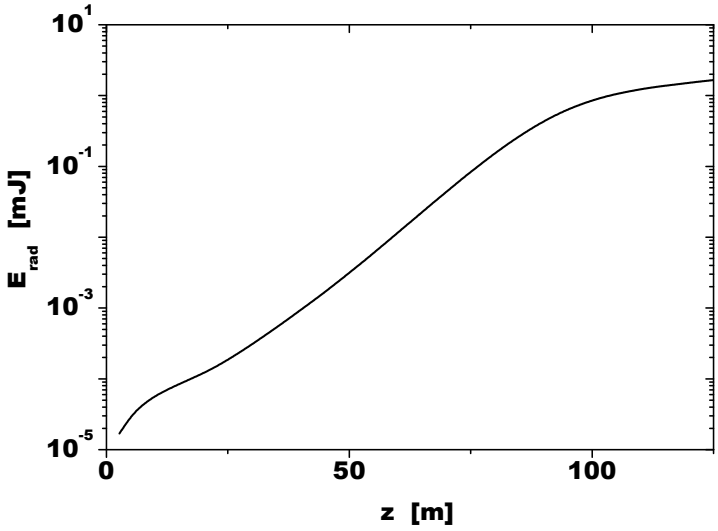

Fig. 7. Average energy in the radiation pulse versus undulator length

the central part of the radiation pulse. The dotted lines in this figure show the initial energy modulation of the electron beam. The temporal structure of the radiation pulse has a clear physical explanation. The FEL process is strongly suppressed in the regions of the electron bunch with large energy chirp, and only regions of the electron bunch with nearly zero energy chirp produce radiation. From a physical point of view each part of the bunch near the local extremum of the energy modulation can be considered as an isolated electron bunch of short duration. At the chosen parameters of the system its duration is about 300 attosecond which is about of coherence time. Thus, it is not surprising that only a single radiation spike is produced by each area near the local extremum. An asymmetry of averaged power (at symmetric energy modulation) is due to the nonsymmetry of the FEL process with respect to the sign and the value of the energy chirp. In particular, spikes related to the negative of energy offset have a higher amplitude. This is a typical nonlinear effect allowing to prolong interaction of the radiation pulse with the electron pulse at the "correct" sign of the energy chirp. The temporal structure of the radiation pulse nearly repeats the temporal structure of the energy modulation. Slight deviations from the periodic structure are also due to the nonsymmetry of the FEL process with respect to the sign of the energy chirp. In particular, spikes related to the negative energy offset slip more forward than those related to the positive energy offset.

Let us turn back to the main subject of our study, i.e. to the production of attosecond pulses. The lower plot in Fig. 8 shows the total radiation spectrum of the radiation pulse. At this scale a signature of the slice energy modulation can hardly be seen. In Fig: 10 we present the tails of the spectrum at an enlarged scale. Each of three clearly visible bumps in the averaged spectrum corresponds to a local extremum of the energy offset shown in Fig. 5. The

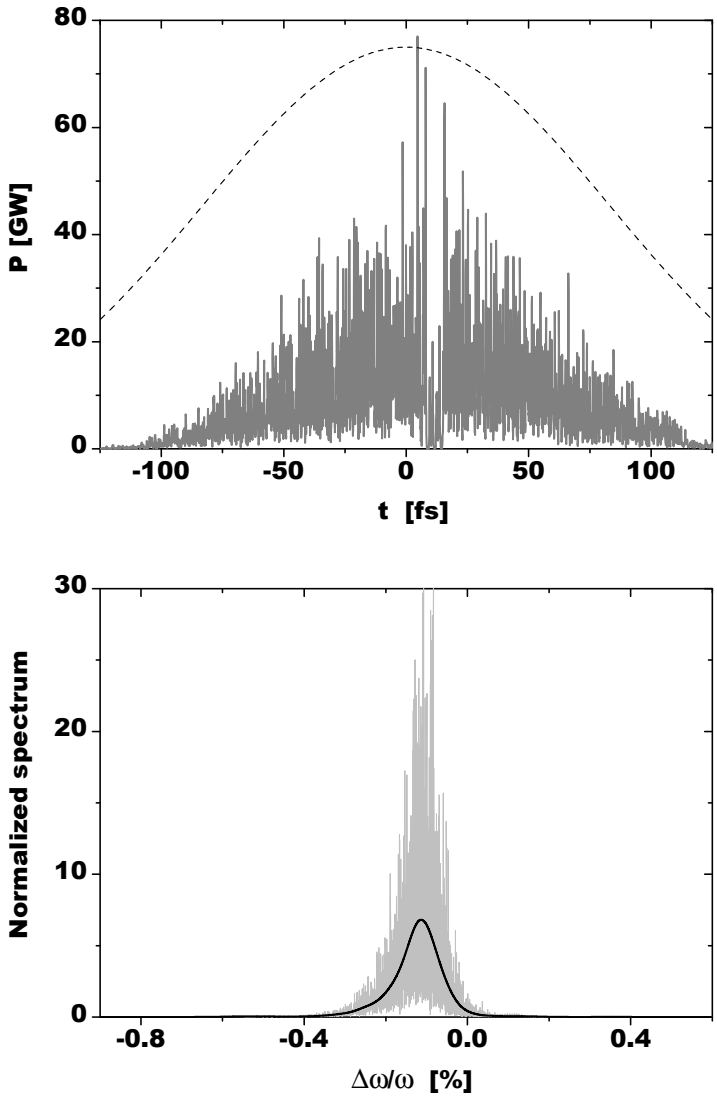

Fig. 8. Temporal (upper plot) and spectral (lower plot) structure of the radiation pulse. Solid line at the lower plot shows averaged spectrum. Undulator length is 120 m

bump marked as M_1 corresponds to the central peak energy offset. The bump M_2 corresponds to the neighboring two positive energy offsets. The bump M_3 comes from the areas of the electron bunch with negative energy offset. The single-shot spectrum (shown as grey line) exhibits an oscillatory behavior near bumps M_2 and M_3. That is due to an interference of two radiation wavepackets with close frequencies coming from different parts of the electron bunch. Other maxima can be hardly distinguished, since they are located within the bandwidth of the main spectrum.

Figures 2, 3, and 10 give a clear idea about separation of the attosecond ra-

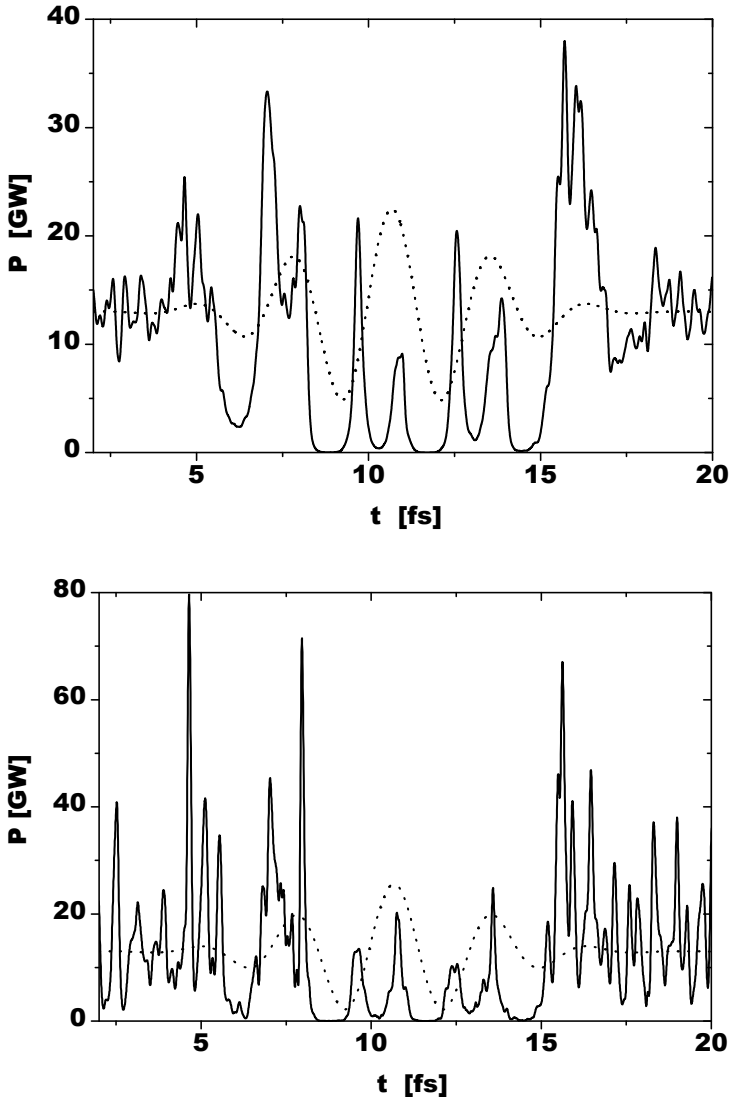

Fig. 9. Averaged (upper plot) and typical single-shot (lower plot) temporal structure of the central part of the radiation pulse. Undulator length is 120 m. Dotted line shows energy modulation of the electron bunch (see Fig. 5)

diation pulses. Positioning of the monochromator to different maxima of the spectrum allows us to select single pulse, or a two pulse sequence of attosecond duration. The calculation involves the following steps. The FEL simulation code produces 3-D arrays for the radiation field in the near zone. This field is recalculated into the far field zone, and is subjected to the Fourier transform. The latter result is convoluted with the reflectivity function of Ge(111) monochromator (see Fig. 6), and is subjected to inverse Fourier transform giving temporal structure of the radiation pulse behind the monochromator.

By selecting the frequency offset of the monochromator to the position marked

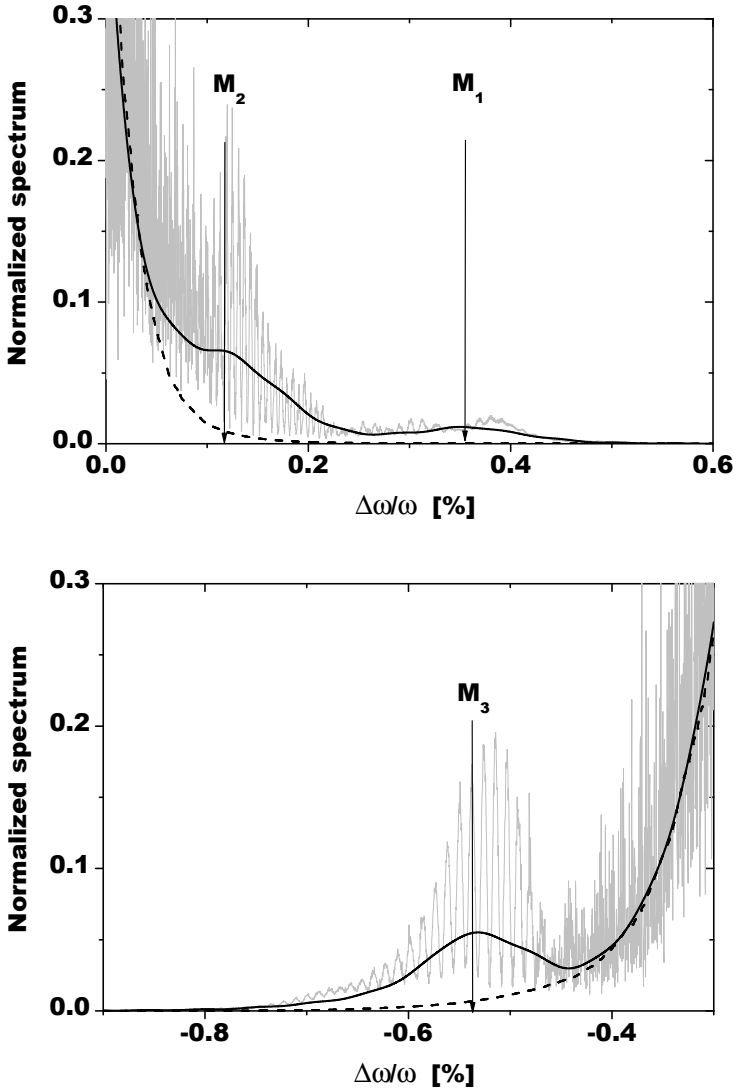

Fig. 10. Spectrum of the radiation pulse produced by modulated electron bunch (gray line). Undulator length is 120 m. Plots show enlarged tails of complete spectrum presented in Fig. 8. Solid line is averaged spectrum. Dashed line is averaged spectrum of nonmodulated electron beam. Mark M_1 shows tuning of monochromator for single pulse selection (see Fig. 11). Marks M_2 and M_3 show tuning of the monochromator for selection of two pulse sequence (see Figs. 12 and 13).

as M_1 in Fig. 10, we select single pulses. Their properties are illustrated with Fig. 11. An analysis of single pulses shows that their pulse duration is about 300 as, the average power has GW-level, and the radiation pulse energy is about a μJ. The larger width of the averaged curve is partially due to shot-to-shot fluctuations of the position of the radiation pulse (a fraction of coherence time). Note that shot-to-shot fluctuations of the radiation energy after monochromator are suppressed significantly due to ultrashort duration of the

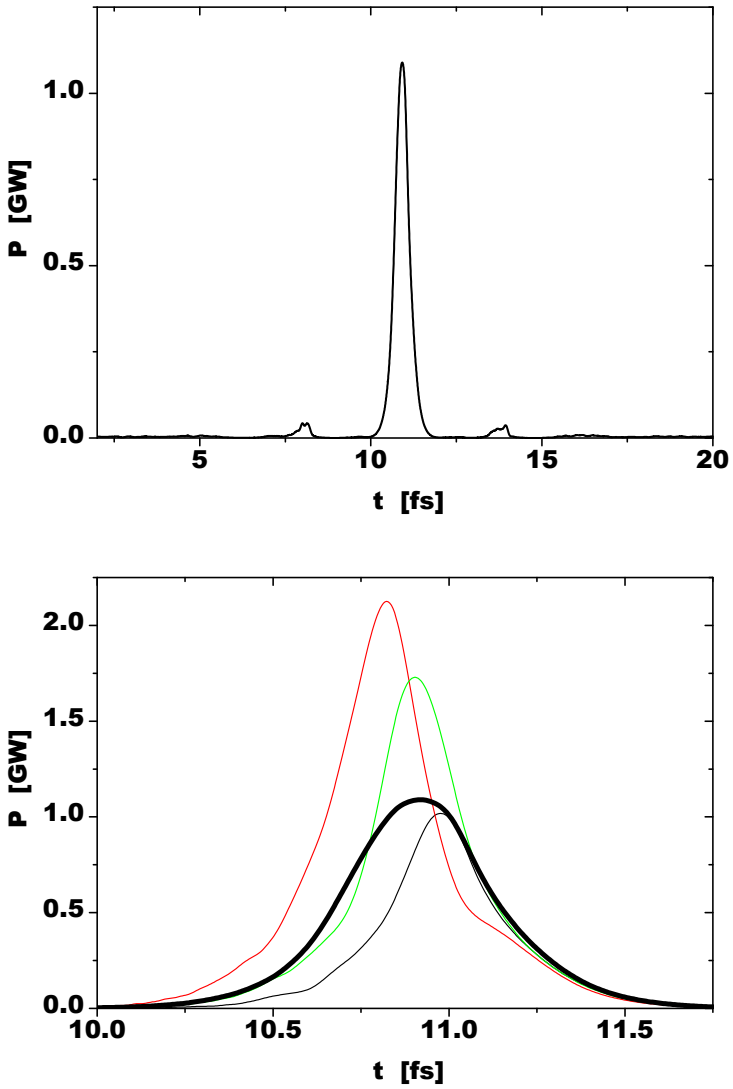

Fig. 11. Temporal structure of the radiation pulse behind monochromator tuned to single spike selection (mark M_1 in Fig. 10). Upper plot shows average over many pulses, and lower plot shows details of single pulses. Bold curve is average over many pulses

lasing fraction of the electron bunch [23]. An advantage of single-pulse selection is the small background from the main radiation pulse due to a large offset from the resonant frequency.

By positioning of the monochromator central frequency to the spectrum bumps M_2 or M_3 one can select a two pulse sequence as illustrated in Figs. 12 and 13. Two pulses are separated by two or one oscillation period of optical laser depending on the choice of the monochromator tuning. Note that due to the statistical nature of the SASE process the time jitter between two pulses is

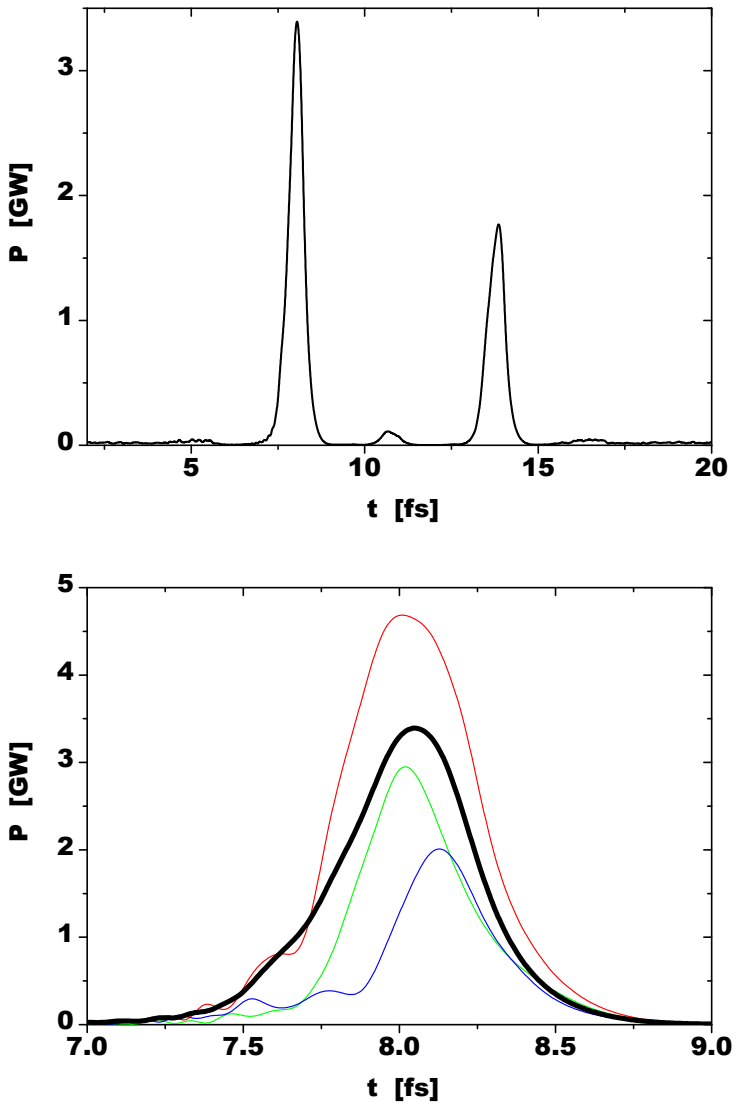

Fig. 12. Temporal structure of the radiation pulse behind monochromator tuned to selection of two pulse sequence (mark M_2 in Fig. 10). Pulse separation is two laser oscillation periods. Upper plot shows average over many pulses, and lower plot shows details of single pulses. Bold curve is average over many pulses

about 200 as, a fraction of the coherence time. One should not wonder that pulse amplitudes differ visibly for the case of pulse separation by one laser oscillation period (see Fig. 12). As mentioned above, this is a typical nonlinear effect related to the sensitivity of the FEL process to the sign and the value of the energy chirp. Although the energy modulation amplitude is the same in both maxima, the shape of the energy chirp is asymmetric.

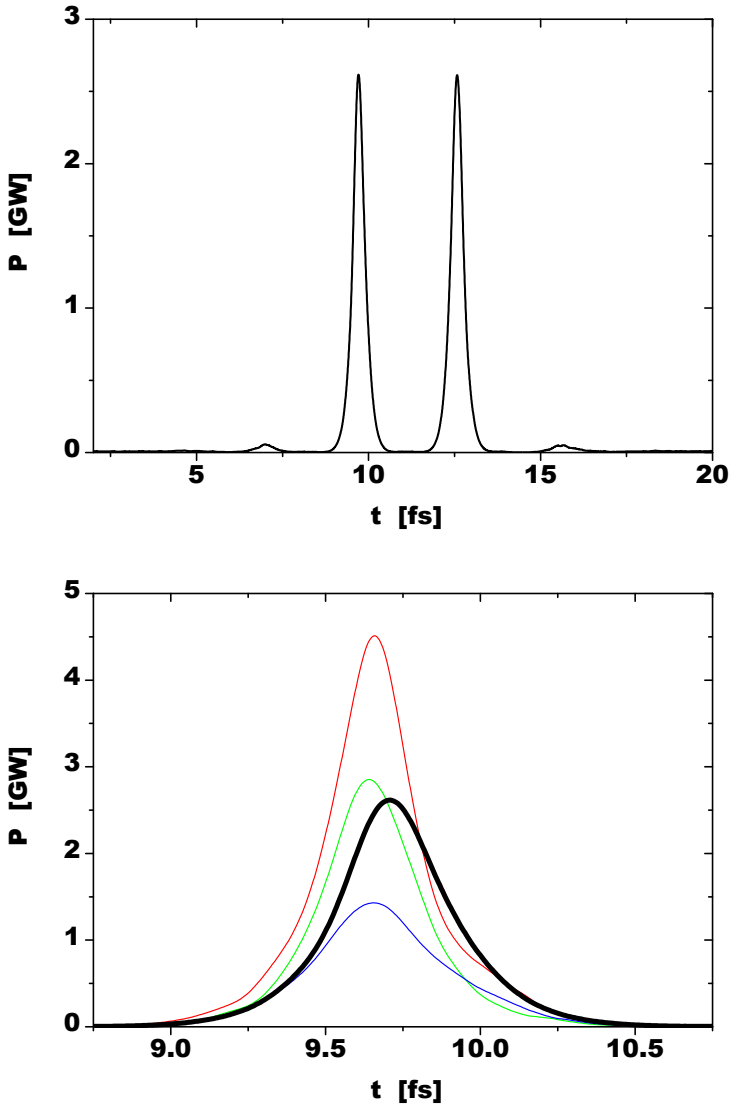

Fig. 13. Temporal structure of the radiation pulse behind monochromator tuned to selection of two pulse sequence (mark M_3 in Fig. 10). Pulse separation is one laser oscillation period Upper plot shows average over many pulses, and lower plot shows details of single pulses. Bold curve is average over many pulses

4 Discussion

Successful operation of the attosecond XFEL requires the fulfillment of several requirements. The requirement that the SASE FEL bandwidth is much less than the separation of the few-cycle-driven frequency offset is of critical importance for the performance of the attosecond XFEL. In this case a crystal monochromator can be used to distinguish the attosecond pulses from the intense SASE pulses. Obviously, this requirement is easier to achieve for high

power optical laser systems. For 800 nm laser radiation and for 0.1 nm output radiation, for example, the peak power of few-cycle laser pulse must be larger than 500-700 GW. This condition can be satisfied by a terawatt-scale sub-10 fs Ti:sapphire laser system which seems feasible.

Our scheme of attosecond X-ray source is based on the assumption that the beam density modulation does not appreciably change as the beam propagates through the energy modulator undulator. When the resonance condition takes place, the electrons with different arrival phases acquire different values of the energy increments (positive or negative), which result in the modulation of the longitudinal velocity of the electrons with the laser frequency. Since the velocity modulation is transformed into a density modulation of the electron beam when, passing the undulator, an additional wakefield exists because of a variation in amplitude density modulation. It is interesting to estimate the amount of bunching produced during the 800 nm undulator pass. An undulator is a sequence of bending magnets where particles with different energies have different path length, $\Delta z = R_{56}\delta E/E$. The net compaction factor of the undulator is given by $R_{56} = 2\lambda_0 N_{\rm w}$, where $\lambda_0 = 800$ nm is the resonance wavelength and $N_{\rm w} = 2$ is the number of undulator periods. An induced correlated energy spread at the exit of (800 nm) undulator is about 0.3%. Therefore, a rough estimate for the induced bunching is $\delta a \simeq (\pi R_{56}/\lambda_0)(\delta E/E) \simeq 3 \times 10^{-2}$. Since this value is much less than unity, we can conclude that density modulation in the 800 nm undulator due to few-cycle-driven energy spread should not be a serious limitation in our case.

The next problem is that of synchronization. Frequency chirp in the XFEL is seeded by positioning a fs optical pulse on the electron bunch. Even when femtosecond pulses from laser system are synchronized to the photoinjector master clock with phase-locking technique, the synchronization of the optical seed laser with the electron pulses to an accuracy of 100 fs is not yet achievable. A more serious problem is the timing jitter of electron and seed laser pulses. The jitter of electron pulses originates in the photoinjector laser system (laser pulse jitter) and in the magnetic bunch compressors (from electron bunch energy jitter). Due to this uncertainty, not every fs optical pulse will produce an attosecond X-ray pulse. Random production of attosecond X-ray pulses needs to be controlled. A basic question at this point is how attosecond X-ray pulses will be identified. Separation of attosecond pulse frequency from the central frequency can be used to distinguish the 300 as pulses from the intense 100 fs pulses. Appearing of X-ray pulses at the frequency offset will indicate that the seed optical pulse is overlapped with the central part of the electron bunch.

Analysis of parameters of an attosecond X-ray source shows that its repetition rate is clearly limited by the value of repetition rate achievable with terawatt-scale sub-10 fs Ti:sapphire laser system having 1-kHz repetition rate [22].

The single-pass scheme considered here is the simplest one. The laser beam, which is essentially unaltered in the electron beam modulation process, is then disposed of. This is not optimum for a couple of reasons. The idea is roughly the following. The attosecond pulse repetition rate can be significantly increased if the laser pulse can be reused, because the laser pulse suffers little loss in energy after each interaction with electron beam. The solution of this problem is a multipass approach (based on reflective optical elements) in which a laser pulse is made to pass through the modulator undulator a finite number of times before being thrown away. In this way, the attosecond pulse repetition rate is increased by increasing the number of laser pulses used.

5 Conclusion

Operation of the proposed scheme was illustrated for the parameters of the European XFEL. Although the present work is concerned primarily for use in the wavelength range around 0.1 nm, its applicability is not restricted to this range, for example 0.15 nm LCLS facility is a suitable candidate for application of attosecond techniques described here. It is important that proposed attosecond scheme is based on the nominal XFEL parameters, and operates in a "parasitic" mode not interfering with the main mode of the XFEL operation. It can be realized with minimum additional efforts. The machine design should foresee the space for installation of modulator undulator and a viewport for input optical system. Many of the components of the required laser system can be achieved with technology which is currently being developed for applications other than the attosecond X-ray source. As a result, a laser system could be developed over the next few years and can meet the XFEL requirements well in advance of XFEL construction schedule.

Acknowledgments

We thank G. Grübel, D. Novikov, E. Weckert for many useful discussions. We thank R. Brinkmann, J.R. Schneider, A. Schwarz, and D. Trines for interest in this work.

References

[1] V. Ayvazyan et al., Phys. Rev. Lett. 88(2002)104802.

[2] V. Ayvazyan et al., Eur. Phys. J. D20(2002)149.

[3] H. Wabnitz et al., Nature 420(2002)482.

[4] SASE FEL at the TESLA Test Facility, Phase 2, DESY print TESLA-FEL 2002-01, Hamburg, 2002.

[5] TESLA Technical Design Report, DESY2001-011, edited by Richard et al., and http://tesla.desy.de.

[6] The LCLS Design Study Group, LCLS Design Study Report, SLAC reports SLAC-R-593 (2002), and http://www-ssrl.slac.stanford.edu/lcls/CDR.

[7] C.B. Schroeder et al., Nucl. Instrum. and Methods A483(2002)89.

[8] E.L. Saldin, E.A. Schneidmiller and M.V. Yurkov, Opt. Commun. 205(2002)385.

[9] S. Reiche, P. Emma, and C. Pellegrini, Nucl. Instrum. and Methods A507(2003)426.

[10] M. Cornacchia, et al., SLAC-PUB-10133, December 2003.

[11] P. Paul, Science 292(2001)1689.

[12] M. Hentchel et al., Nature 414(2001)509.

[13] L.H. Yu et al., Science 289(2000)932.

[14] W. Fawley et al., Preprint LBNL-52596, LBNL, Berkeley, 2003.

[15] A. Zholents and W.M. Fawley, Preprint LBNL-54084, LBNL, Berkeley, 2003.

[16] E.L. Saldin, E.A. Schneidmiller and M.V. Yurkov, Opt. Commun. 202(2002)169.

[17] E.L. Saldin, E.A. Schneidmiller and M.V. Yurkov, Opt. Commun. 212(2002)377.

[18] TESLA Technical Design Report, Supplement, DESY2002-167, edited by R. Brinkmann et al., and http://tesla.desy.de.

[19] E.L. Saldin, E.A. Schneidmiller and M.V. Yurkov, The physics of Free Electron Lasers, Springer, Berlin-Heidelberg-New-York, 1999.

[20] T. Brabec and F. Krausz, Rev. Mod. Phys., 72(2000)545.

[21] E.L. Saldin, E.A. Schneidmiller and M.V. Yurkov, Nucl. Instrum. and Methods A429(1999)233.

[22] A. Baltushka et al., Nature, 421(2003)611.

[23] E.L. Saldin, E.A. Schneidmiller and M.V. Yurkov, Nucl. Instrum. and Methods A507(2003)101.